reactions

MDPI

Article

Formation of OH Radicals on $BiVO_4$–TiO_2 Nanocomposite Photocatalytic Film under Visible-Light Irradiation: Roles of Photocatalytic Reduction Channels

Shizu Terao and Yoshinori Murakami *

Department of Materials Engineering, National Institute of Technology, Nagaoka College, Niigata 940-8532, Japan
* Correspondence: murakami_mb@nagaoka-ct.ac.jp

Abstract: In this study, we investigated the effects of H_2O_2 addition on OH radical formation on the surfaces of visible-light-irradiated $BiVO_4$–TiO_2 nanocomposite photocatalysts. Additionally, we examined the possible roles of OH radicals formed by the reduction reaction of H_2O_2 on the visible-light-irradiated surfaces of photocatalytic $BiVO_4$–TiO_2 nanocomposites. The $BiVO_4$–TiO_2 nanocomposite photocatalysts were prepared by mixing a $BiVO_4$ photocatalytic film with commercially available semiconductor particulate TiO_2 photocatalysts. By removing oxygen gas from the photocatalytic reactor, the effects of oxygen molecules on OH radical formation during the visible-light irradiation of $BiVO_4$–TiO_2 nanocomposite photocatalysts were examined. During visible-light irradiation, $BiVO_4$ and $BiVO_4$–TiO_2 photocatalysts play different roles in OH radical formation because of two characteristic reduction reaction channels: (a) the direct reduction of H_2O_2 on photocatalytic surfaces and (b) the indirect reduction reaction of H_2O_2 by superoxide radical anions (O_2^-).

Keywords: OH radical; $BiVO_4$; photocatalysis; reduction; H_2O_2

check for updates

Citation: Terao, S.; Murakami, Y. Formation of OH Radicals on $BiVO_4$–TiO_2 Nanocomposite Photocatalytic Film under Visible-Light Irradiation: Roles of Photocatalytic Reduction Channels. *Reactions* **2024**, *5*, 98–110. https://doi.org/10.3390/reactions5010004

Academic Editor: Hugo de Lasa

Received: 1 November 2023
Revised: 16 December 2023
Accepted: 22 December 2023
Published: 22 January 2024

1. Introduction

Semiconductor photocatalysis has attracted increasing attention because of its diverse applications, including water-splitting reactions for solar energy conversion and the removal of organic pollutants from aqueous solutions or gas phases. Owing to its relatively small optical band gap of approximately 2.4 eV [1,2], monoclinic bismuth vanadate (*m*-$BiVO_4$) has been recognized as a promising semiconductor photocatalyst with high photocatalytic activity in the evolution of oxygen and high visible-light absorption capability. Since the discovery of $BiVO_4$, many new Bi-containing visible light-induced photocatalysts have been reported, including Bi_2WO_6 [3], Bi_2O_3 [4], $CaBi_2O_4$ [5], $BiCu_2PO_6$ [6], and Bi_2MoO_6 [7]. However, $BiVO_4$ is known to have poor carrier transport properties owing to its short electron diffusion length [8,9]. As a result, several attempts have been made to improve the separation of photogenerated electron–hole pairs and increase the charge carrier lifetime in $BiVO_4$ photocatalysts by coupling them with other metal-oxide semiconductors with appropriate band potentials.

Among visible-light-responsive $BiVO_4$ photocatalysts, several studies have been conducted on $TiO_2/BiVO_4$ heterojunction or nanocomposite photocatalysts, often in combination with ultraviolet-responsive photocatalysts. Hu et al. [10] reported the enhanced heterogeneous photocatalytic oxidation of gaseous benzene using $TiO_2/BiVO_4$ heterojunction photocatalysts under visible-light irradiation ($\lambda > 450$ nm). Zhang et al. [11] reported higher decolorization rates of rhodamine B, and Wetchakun et al. [12] reported the decolorization of methylene blue under solar light irradiation. Both of these studies attributed the higher photocatalytic activity to the increased rate of separation of the photogenerated charge carriers. Son et al. [13] also observed that the photocatalytic degradation rate of gaseous ethylene for $BiVO_4$–TiO_2 (P25) nanocomposites under visible-light irradiation was significantly higher than that for both bare $BiVO_4$ and bare TiO_2 (P25)

particles. They also attributed this higher photocatalytic activity to the charge transfer between the n-type $BiVO_4$ and n-type TiO_2 (P25). To identify highly efficient materials for water oxidation, several researchers [14–16] fabricated nanostructured composite electrodes of $BiVO_4$–TiO_2, which exhibited enhanced photocurrent efficiencies under visible light irradiation. Polo et al. [17] used an electron acceptor probe for methyl viologen and directly observed the electron transfer from photoexcited $BiVO_4$ to the TiO_2 conduction band in a $TiO_2/BiVO_4$ heterojunction. They observed the pronounced ability of the $TiO_2/BiVO_4$ heterojunction to reduce methyl viologen, indicating enhanced charge separation resulting from the transfer of photoexcited electrons in $BiVO_4$ to the conduction band of TiO_2 under visible-light irradiation.

Although improvements in the charge separation efficiency of $TiO_2/BiVO_4$ heterojunction photocatalysts have been reported, there is a lack of research clarifying the influence of OH radical formation by the heterojunction under visible-light-responsive $BiVO_4$ in combination with other semiconductor photocatalysts. Kohtani et al. [18] investigated the photodegradation reactions of polycyclic aromatic hydrocarbons over $BiVO_4$ and Ag-$BiVO_4$ and indicated the crucial role of OH radicals in the degradation of polycyclic aromatic hydrocarbons. Zhang et al. [19] investigated the yield of OH radicals generated on WO_3 and $BiVO_4$ photocatalysts under 470 nm LED irradiation. They confirmed that the yield of OH radicals generated on the WO_3 photocatalyst was comparable to that on anatase TiO_2, whereas the yield of OH radicals on $BiVO_4$ was much lower.

Although various types of TiO_2 photocatalysts are commercially available, there is no clear understanding of their photocatalytic activities or characteristic charge carrier behaviors. In particular, crystal phase and primary particle size have some influence on the charge carrier dynamics of TiO_2 particles. However, only a few studies have been carried out using commercially available TiO_2 powders. The present study examined OH radical formation on $BiVO_4$–TiO_2 nanocomposite photocatalysts prepared by mixing $BiVO_4$ photocatalytic films with commercially available semiconductor particulate TiO_2 photocatalysts. We also explored the possible roles of OH radicals formed by the reduction reaction of H_2O_2 on the surfaces of these nanocomposite photocatalysts.

2. Experimental Section

2.1. Materials

$Bi(NO_3)_3{\cdot}5H_2O$ (0.2–1.0 mmol) and NH_4VO_3 (0.2–1.0 mmol) were dissolved in 10 mL HNO_3 solution (1.0 mol/L) and stirred for 5 min under ambient air, which was followed by 1 min of ultrasonic irradiation. After the color of the mixed solution turned orange, it was mixed with commercially available TiO_2 particles and stirred for 5 min. The orange suspension containing the TiO_2 particles was then ultrasonicated for approximately 5 min and used as a solution for dip-coating the quartz glass. $BiVO_4/TiO_2$ nanocomposite photocatalytic films were obtained by dip-coating quartz glass (diameter: 30 mm) at a rate of approximately 60 cm/min. The obtained nanocomposite films were then annealed in air for 5 min at approximately 600 K (~330 °C), and these procedures were repeated three times. Finally, the films were annealed again at approximately 600 K (~330 °C) for 1 h. The TiO_2 powders used in this study were generous gifts from Ishihara Sangyo (ST-01), Showa Titanium (F-1, F-2), Degussa (P25), and Tayca (AMT-100, AMT-600, MT-150A, and MT-500B), and were used without any modification. TiO_2 powders purchased from Wako Co., Ltd. (Tokyo, Japan) (purity $\geq$ 99.9%) were used after further purification. The primary particle sizes and anatase ratios of commercially available TiO_2 powders are listed in Table 1. Analytical grade $Bi(NO_3)_3{\cdot}5H_2O$ and NH_4VO_3 were used without further purification. The crystal form of the prepared thin film was analyzed by X-ray diffraction (XRD, Rigaku, Ultima IV) using a Cu-Kα radiation source (λ = 1.541 Å). Characteristic XRD peaks corresponding to the diffraction patterns of the monoclinic phase of $BiVO_4$ were observed, along with additional peaks attributed to the TiO_2 photocatalytic particles. The thickness of the films was examined using scanning electron microscopy (SEM). We confirmed that all photocatalytic films prepared in this study had a thickness of approxi-

mately 50 μm (see Figure 1a). Elemental analysis of the film surface was performed using energy-dispersive X-ray spectroscopy (EDS) with a thermal emission scanning electron microscope (FESEM, JEOL, JSM-IT200LA) operating at 15 kV, as shown in Figure 1b. Subsequently, the homogeneous distribution of $BiVO_4$ on the photocatalytic TiO_2 particles was confirmed. In other words, the images presented in Figure 1 confirmed that TiO_2 particles were attached to the glass plate in aggregated particulate forms; among these TiO_2 particles, $BiVO_4$ photocatalysis served as a mediator for capturing visible light between the TiO_2 particles attached to the glass plate. The Bi/Ti atomic ratios of the photocatalytic films were estimated using EDS and are used in the present discussion. Finally, the optical absorption of the $BiVO_4$–TiO_2 films was examined using diffuse reflectance spectroscopy with an integrating sphere attached to a UV-VIS-NIR spectrometer (JASCO. V-770). It was confirmed that the optical absorption of these films extended to the visible region because of the absorption of $BiVO_4$ photocatalysts.

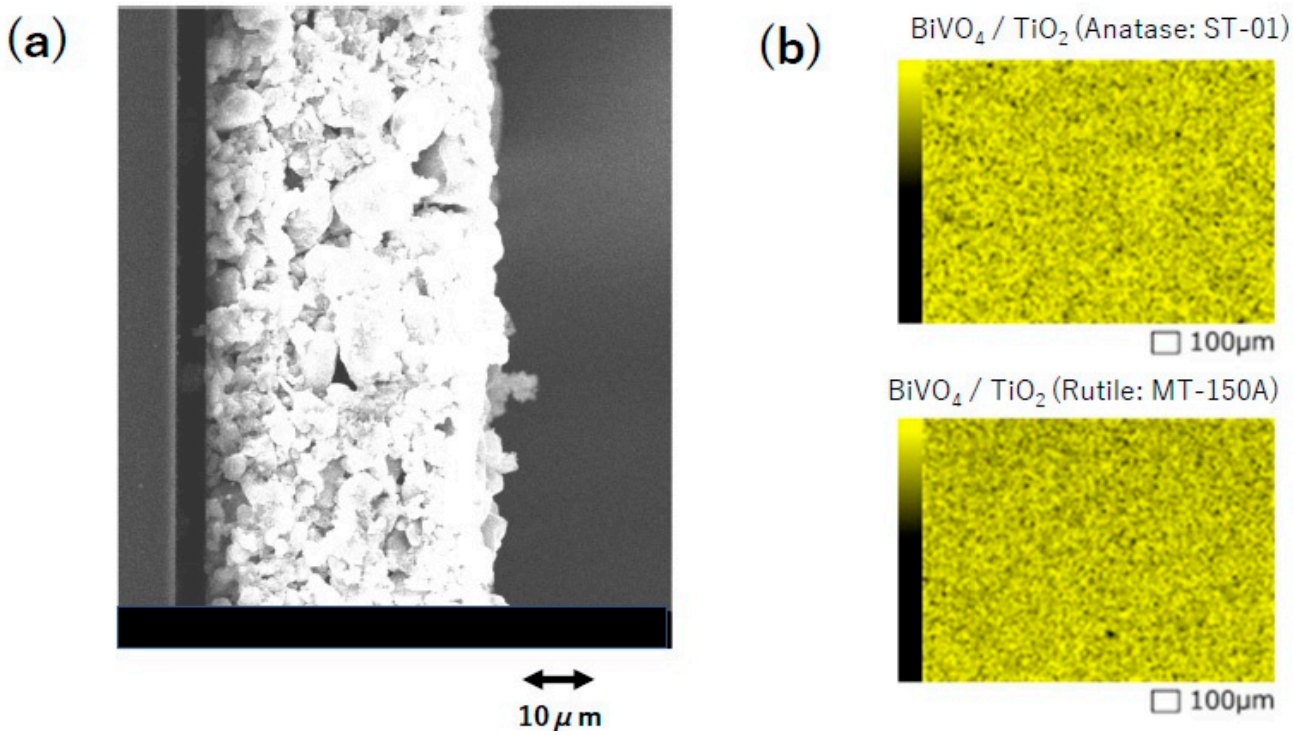

Figure 1. (**a**) Scanning electron micrograph of the cross-section of a $BiVO_4$–TiO_2 (ST-01) nanocomposite film. (**b**) Energy-dispersive spectroscopy (EDS) element mapping image of $BiVO_4$–TiO_2 nanocomposite films containing ST-01 (anatase, upper figure) and MT-150A (rutile, lower figure) TiO_2 powders.

Table 1. Primary particle sizes and anatase ratios for TiO_2 powders used in the present study. All data regarding the TiO_2 powders were obtained from the suppliers. BET surface area measuremnents were taken from references [20–24].

Name	Anatase Content (%)	Rutile Content (%)	Primary Particle Size (nm)	BET Surface Area (m^2 g^{-1})	Supplier
ST-01	100	0	7	320 [21,22]	Ishihara Sangyo
F1	90	10	50	26 [23]	Showa Titanuim
F2	60	40	40	-	Showa Titanuim
P25	70 [20]	30	21	32 [21], 49 [22]	Degussa

Table 1. *Cont.*

Name	Anatase Content (%)	Rutile Content (%)	Primary Particle Size (nm)	BET Surface Area (m^2 g^{-1})	Supplier
AMT-100	100	0	6	6 [21]	Tayca
AMT-600	100	0	30	30 [21], 49 [22]	Tayca
MT-150A	0	100	15	88 [22]	Tayca
MT-500B	0	100	35	38 [23]	Tayca
Wako	100	0	41.5	8.3 [24]	Wako Chemicals

2.2. Fluorescence Probe Detection of OH Radicals

In this study, OH radicals were detected using the coumarin fluorescence probe technique [25,26]. Briefly, this technique was used to detect 7-hydroxycoumarin, which emits stronger fluorescence than the parent coumarin molecule. By monitoring the fluorescence intensity of 7-hydroxycoumarin at approximately 450 nm (excitation wavelength of 350 nm), the relative yield of OH radicals formed by the photocatalytic reaction of $BiVO_4/TiO_2$ nanocomposite photocatalytic films was estimated. The $BiVO_4/TiO_2$ nanocomposite photocatalytic films were placed in a 0.15 mM coumarin solution and were irradiated with LED light at 470 nm (Asahi Spectra, CL-H1-470) with an average power of approximately 50 mW/cm^2. After visible-light irradiation, OH radicals were measured using the coumarin fluorescence probe method after sampling the LED-light-irradiated 0.15 mM coumarin solution. All experiments using the coumarin fluorescence probe technique were performed more than three times to confirm reproducibility, and the average value was used as the present result.

3. Results and Discussion

3.1. Detection of OH Radicals Formed by the $BiVO_4$–TiO_2 Photocatalyst

Figure 2a shows the fluorescence spectra obtained by the visible light irradiation of the $BiVO_4$–TiO_2 (anatase: ST-01) and $BiVO_4$–TiO_2 (rutile: MT-150A) nanocomposite photocatalysts. As shown in Figure 2a, the fluorescence of 7-hydroxycoumarin was observed at approximately 450 nm by the visible light irradiation of the $BiVO_4$–TiO_2 photocatalyst. Therefore, the formation of OH radicals on the visible-light-irradiated $BiVO_4$–TiO_2 photocatalyst was confirmed. Next, we investigated the effect of the amount of TiO_2 particles on the yield of OH radicals formed by the visible-light-irradiated $BiVO_4$–TiO_2 nanocomposite photocatalysts with the irradiation time fixed at 1 h. The results are presented in Figure 2b. As shown in Figure 2b, the fluorescence intensity of 7-hydroxycoumarin increased with an increase in the amount of TiO_2 particles in the $BiVO_4$–TiO_2 nanocomposite photocatalysts, which was irreversible for commercially available TiO_2 powders, such as ST-01 (anatase), AMT-100 (anatase), MT-150A (rutile), and MT-500B (rutile). These results can be attributed to the suppression of the recombination of photoexcited electrons and holes in $BiVO_4$. This is due to the enhanced transfer of photoexcited electrons from the visible-light-irradiated $BiVO_4$ thin film to TiO_2 particles, which is caused by the increase in the amount of TiO_2 particles in the $BiVO_4$ thin films. However, Figure 2b also shows differences in electron transfer and the suppression of charge recombination between TiO_2 particles. This indicates that the number of OH radicals formed on the TiO_2 particles of ST-01(anatase) and AMT-100 (anatase) appeared to be much higher than those on the TiO_2 particles of MT-150A (rutile) and MT-500B (rutile), despite having the same amount of TiO_2 in the $BiVO_4$–TiO_2 nanocomposite photocatalysts. To further investigate the differences in the charge transfer rates from $BiVO_4$ to TiO_2 particles (ST-01 (anatase), AMT-100 (anatase), MT-150A (rutile), and MT-500B (rutile)), we studied the OH radical formation on the visible-light-irradiated $BiVO_4$ nanocomposite photocatalytic films with various other commercially available TiO_2 particles. Figure 3 shows the relationship between the fluorescence intensity of 7-hydroxycoumarin and primary particle size of TiO_2. As shown in Figure 3, the number

of OH radicals formed through the photoexcited electron transfer from the visible-light-irradiated $BiVO_4$ thin film to TiO_2 particles was independent of the particle size and crystal phase of TiO_2 except for the two commercially available TiO_2 particles, ST-01 and AMT-100, which have a very small primary particle size of less than 10 nm. Dibbell et al. [27] reported the dependence of electron transfer on the distance between CdS quantum dots and TiO_2 nanoparticles. They concluded that the electron injection yield decreases with increasing the chain length of bifunctional mercaptoalkanoic acid and interparticle separation. For the plasmonic excitation of Au−TiO_2 photocatalysts, Du et al. [28] reported that for all TiO_2 nanoparticle diameters, the plasmon-induced electron injection yields were almost the same within the experimental error with efficiencies of approximately 20–50%. However, the charge recombination decay was strongly dependent on the particle diameter of TiO_2. Our results are similar to those of the plasmon-induced electron injection yields observed in the plasmonic excitation of Au−TiO_2 photocatalysts, which showed almost the same yields for all TiO_2 nanoparticle diameters. However, higher yields of OH radicals were obtained for the two commercially available TiO_2 particles, ST-01 and AMT-100, which have small primary diameters. The reason for this has not been clarified yet. Liu et al. [29] investigated the effect of particle size on the liquid-phase photooxidation of phenol using nanometer-sized TiO_2 crystals. They observed that the reaction rate constants for the photocatalytic decomposition of phenol were maximized when the anatase TiO_2 particles were approximately 10 nm. The optimal particle size for the photocatalytic oxidation of phenol is attributed to the competing effects of volume recombination, surface recombination, migration of photogenerated electrons and holes, light absorption, defects, and surface area. Similar effects may be important in our present results, where nanocomposites of the $BiVO_4$ thin films with two commercially available TiO_2 particles, ST-01 and AMT-100, exhibit a higher quantum yield of OH radicals.

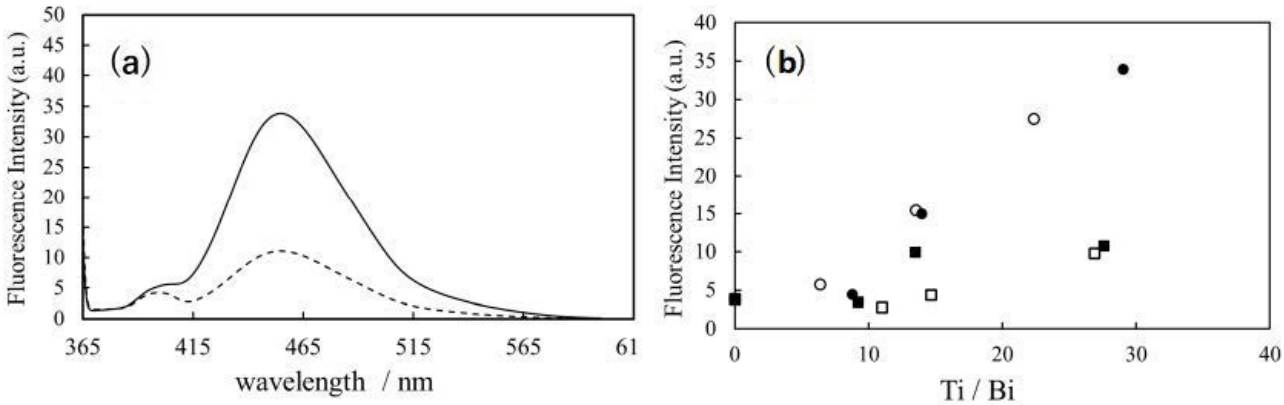

Figure 2. (**a**) Fluorescence spectra of 7-hydroxycoumarin obtained after 1 h visible LED light irradiation of the $BiVO_4$–TiO_2 (anatase: ST-01) (solid line) and $BiVO_4$–TiO_2 (rutile: MT-150A) (dashed line) nanocomposite photocatalysts at 470 nm. (**b**) Dependence of the Ti/Bi ratio in the $BiVO_4$–TiO_2 nanocomposite film on the fluorescence intensity of 7-hydroxycoumarin formed during 1 h visible LED light irradiation at 470 nm. This $BiVO_4$–TiO_2 nanocomposite film was placed in a 0.15 mM coumarin aqueous solution. The commercially available TiO_2 particles used for the $BiVO_4$–TiO_2 nanocomposite film were ST-01; anatase (●), AMT-100; anatase (○), MT-150A, rutile (■), and MT-500B, rutile (□). For all these experiments, the excitation wavelength was set to 350 nm. Additionally, the Ti/Bi ratios estimated through the EDS measurements were used in the figure.

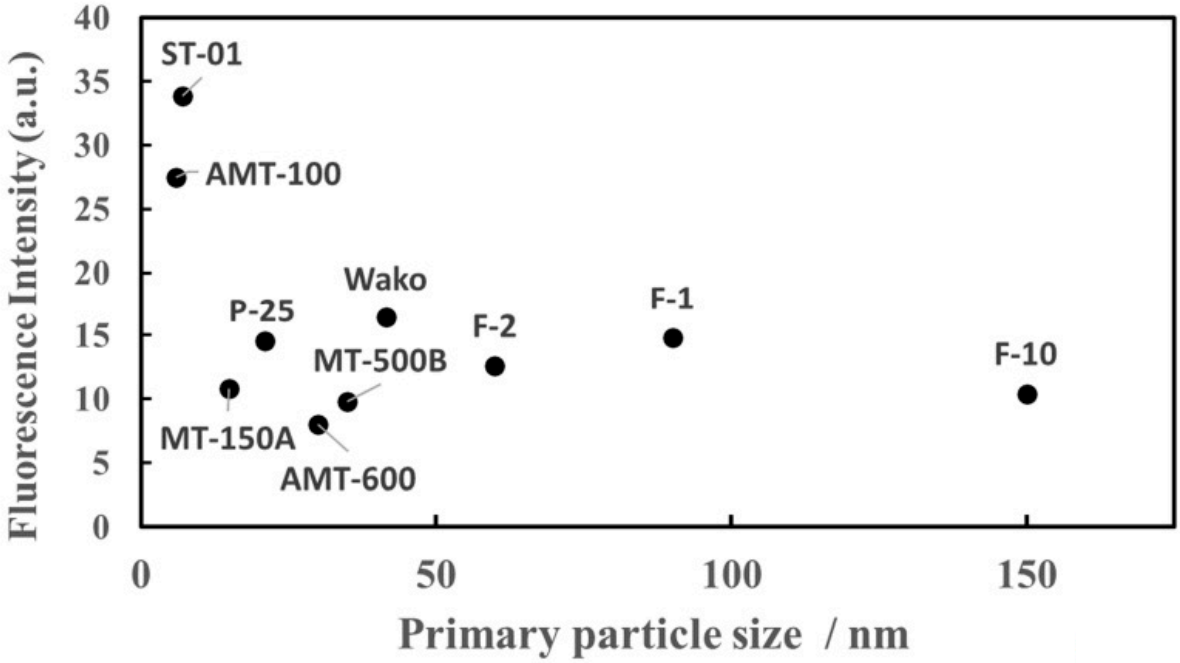

Figure 3. Relationship between the fluorescence intensity of 7-hydroxycoumarin formed during 1-h visible LED light irradiation at 470 nm and the primary particle sizes of the TiO_2 particles. For this purpose, the $BiVO_4$–TiO_2 nanocomposite film (Ti/Bi ratio was fixed at 20:1) was placed in a 0.15 mM coumarin aqueous solution. Various commercially available TiO_2 powders listed in Table 1 were used. The names of the commercially available TiO_2 powders have also been indicated in the above figure, and their primary particle sizes were taken from Table 1. For all these fluorescence measurements, the excitation wavelength was set to 350 nm.

3.2. Effects of H_2O_2 Addition for OH Radical Formation by the Visible Light Irradiated $BiVO_4$–TiO_2 Photocatalyst

To understand the potential roles of OH radical formation through the photocatalytic reduction of H_2O_2 on $BiVO_4$–TiO_2 nanocomposite photocatalysts, we examined the effects of H_2O_2 addition on the amount of OH radicals formed on the surfaces of photocatalytic $BiVO_4$ films mixed with several commercially available TiO_2 particles (Anatase: ST-01, Wako, Rutile: MT-150A, MT-500B) under visible-light irradiation. Serpone et al. [20,30] proposed the formation of OH radicals via the photocatalytic reduction of H_2O_2 on the TiO_2 surface. Li et al. [31] investigated the decomposition of H_2O_2 on TiO_2 surfaces under visible-light irradiation. They observed OH radicals formed on the TiO_2 surfaces by the photocatalytic decomposition of H_2O_2 under visible light irradiation and supported the mechanism reported by Serpone et al. [20,30]. Figure 4 shows that the amount of OH radicals increased with an increase in H_2O_2 concentration in the 0.15 mM coumarin solution containing the $BiVO_4$–TiO_2 nanocomposite photocatalytic film. These results indicate that OH radicals are generated during the photocatalytic reduction of H_2O_2 on the surfaces of $BiVO_4$ and TiO_2. It was also confirmed that the number of OH radicals increased with an increase in the concentration of H_2O_2, irrespective of the type of crystal phase of TiO_2 (anatase or rutile) in the $BiVO_4$–TiO_2 nanocomposite photocatalytic film. These results are similar to those obtained in a previous study by Hayashi et al. [32], in which they used a visible-light-induced plasmonic Au–TiO_2 photocatalyst. They also found that OH radicals were generated only in the presence of H_2O_2 by the visible-light plasmonic excitation of the Au–TiO_2 photocatalyst. In addition, they observed an increase in the number of OH radicals in various crystal phases of TiO_2 (anatase or rutile) by adding H_2O_2 to the Au–TiO_2 plasmonic photocatalyst. From these results, they concluded that OH radicals were formed by the photocatalytic reduction of H_2O_2 on the surface of TiO_2 by electrons in the TiO_2 conduction band. These electrons migrate from the plasmonically excited Au

nanoparticles. In contrast, Hirakawa et al. [33] observed a decrease in OH radical formation on the anatase form of TiO_2 photocatalytic powders because of the addition of H_2O_2 to the TiO_2 suspension. Although the reasons for such different trends—the increase or decrease in the amount of OH radicals between the photocatalytic reactions of visible-light-irradiated $BiVO_4$–TiO_2 nanocomposite or plasmonic Au–TiO_2 photocatalysts and UV-irradiated TiO_2 photocatalysts—have not yet been clarified, it may be attributed to the surface conditions and the presence of holes in TiO_2.

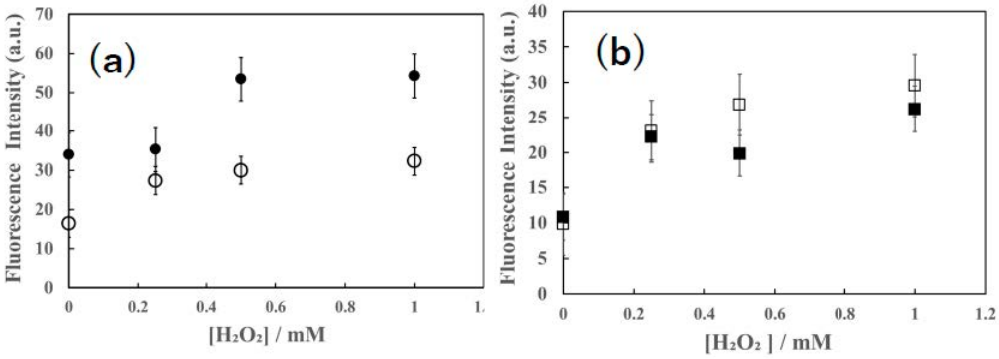

Figure 4. Dependence of H_2O_2 concentration on the fluorescence intensity of 7-hydroxycoumarin formed by the 1 h visible LED light irradiation (470 nm) of the $BiVO_4$–TiO_2 nanocomposite photocatalytic film suspended in a 0.15 mM coumarin aqueous solution. (**a**) Anatase form of TiO_2 particles: ST-01 (●), Wako (○). (**b**) rutile form of TiO_2 particles: MT-150A (■), MT-500B (□). Experiments were repeated more than three times, and the error bars for the data are also illustrated in the figure. For these experiments, the Ti/Bi ratio for the $BiVO_4$–TiO_2 nanocomposite film used was fixed at 20:1, and the excitation wavelength was set to 350 nm.

To further investigate the relative roles of $BiVO_4$ and TiO_2 in OH radical formation at the reduction site of the $BiVO_4$–TiO_2 nanocomposite photocatalysts, we examined the increase in the number of OH radicals formed on the $BiVO_4$ thin-film photocatalysts upon the addition of H_2O_2. The results are shown in Figure 5. First, an increase in the number of OH radicals was observed on the $BiVO_4$ thin-film photocatalyst under visible-light irradiation. To confirm the differences in the excitation wavelengths of $BiVO_4$, we also investigated the OH radical formation on a bare $BiVO_4$ thin-film photocatalyst under UV light irradiation. An increase in the number of OH radicals was observed on the $BiVO_4$ thin-film photocatalyst under UV irradiation, which was similar to the results for the visible-light-irradiated $BiVO_4$ thin-film photocatalyst. However, the increase in the number of OH radicals on the UV-irradiated $BiVO_4$ thin-film photocatalyst was much larger than that in the non-irradiated $BiVO_4$ thin-film photocatalyst. This indicates that the OH radicals were formed via photocatalytic reduction at the conduction band of the $BiVO_4$ thin-film photocatalyst. We speculated that the increase in OH radical formation for the UV-irradiated $BiVO_4$ thin-film photocatalyst was large because the excitation energy of UV light is higher than that of visible light. Furthermore, we observed that the amount of OH radicals formed by the visible-light irradiation of the bare $BiVO_4$ thin-film photocatalyst was much smaller than that formed by the visible-light irradiation of the $BiVO_4$–TiO_2 nanocomposite thin film photocatalyst (Figure 5). Zhang et al. [19] and Nakabayashi et al. [34] have already reported the generation of OH radical on the $BiVO_4$ photocatalyst by photocatalytic water oxidation. The present results indicate that OH radical formation by water oxidation at the surface of the $BiVO_4$ photocatalyst increased when the photocatalytic films were mixed with commercially available TiO_2 photocatalytic powders. This supports our conclusion that the photoexcited electron transfer from the visible light-irradiated $BiVO_4$ thin film to TiO_2 particulates, along with the suppression of the recombination reaction of photoexcited electrons and holes in $BiVO_4$, resulted in an increased amount of OH radicals formed by water oxidation at the $BiVO_4$ surface in the $BiVO_4$–TiO_2 nanocomposite thin film.

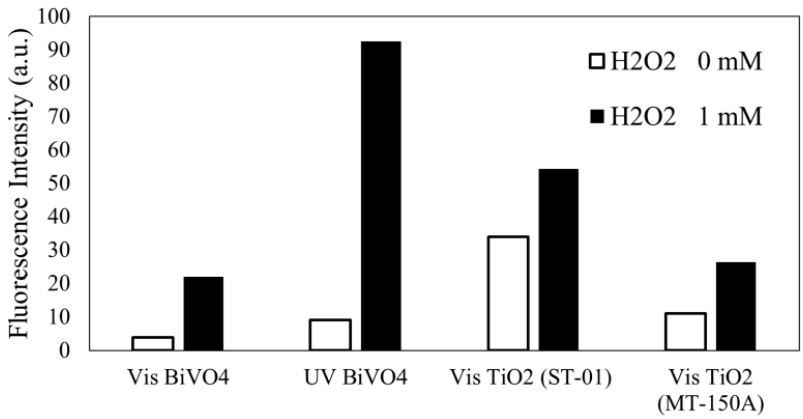

Figure 5. Fluorescence intensity of 7-hydroxycoumarin formed by the 1 h visible LED light irradiation (470 nm) of the bare $BiVO_4$ photocatalytic film (the first left bar) and the 1 h UV LED light irradiation (350 nm) of the bare $BiVO_4$ (the second left bar) and $BiVO_4$–TiO_2 (Anatase: ST-01, Anatase: MT-150A, Rutile) nanocomposite photocatalytic films (the second right and right bars). These films were suspended in 0.15 mM coumarin aqueous solutions with 1 mM H_2O_2 (■) and without H_2O_2 (□). The commercially available TiO_2 particles (Anatase: ST-01, Anatase: MT-150A, Rutile) listed in Table 1 were used. For all measurements, the Ti/Bi ratio for the $BiVO_4$–TiO_2 nanocomposite film used was fixed at 20:1. The excitation wavelength for the fluorescence measurements was set to 350 nm.

Figure 5 shows that H_2O_2 addition increased the fluorescence intensity of 7-hydroxycoumarin for all the $BiVO_4$–TiO_2 photocatalytic films and bare $BiVO_4$ photocatalytic films. As shown in Figure 5, H_2O_2 addition also increased the amount of OH radicals on both the $BiVO_4$–TiO_2 nanocomposite film and $BiVO_4$ photocatalytic thin film under visible light irradiation. However, the ratio of increase in the amount of OH radicals on the $BiVO_4$–TiO_2 nanocomposite photocatalysts was smaller than that on the $BiVO_4$ thin film after H_2O_2 addition under visible light irradiation (Figure 5). The variation in the ratio of the increase between the visible light-irradiated $BiVO_4$–TiO_2 nanocomposite film and $BiVO_4$ thin film may be attributed to their different abilities for OH radical formation. During the photocatalytic reduction reaction, the $BiVO_4$ photocatalytic surface may exhibit a greater ability for OH radical formation than the TiO_2 surface. However, this is not true because the conduction band of $BiVO_4$ is more positive than that of TiO_2. When $BiVO_4$ is in contact with TiO_2, its conduction band becomes more negative than that of TiO_2 because of the matching Fermi levels of both semiconductors. The band shifts of $BiVO_4$ and TiO_2 when $BiVO_4$ and TiO_2 are in contact with each other were also proposed by Wetchakun et al. [12] and Song et al. [13]. Furthermore, Shi et al. [35] and Wang et al. [36] reported band shifts of $BiVO_4$ and TiO_2 such that the conduction band edge of $BiVO_4$ became more negative than that of TiO_2. Our present experimental observation, indicating that the ability of OH radical formation on the TiO_2 photocatalytic surface was smaller than that on the $BiVO_4$ surface for the visible light-irradiated $BiVO_4$–TiO_2 nanocomposite films, could be evidence for the matching Fermi levels of the $BiVO_4$ film and TiO_2 particles in the $BiVO_4$–TiO_2 nanocomposite thin film. Thus, the conduction band edge of $BiVO_4$ became more negative than that of TiO_2 even when the $BiVO_4$ film was in contact with commercially available TiO_2 particles.

3.3. Influence of Oxygen on OH-Radicals Formation on the $BiVO_4$ and the $BiVO_4$–TiO_2, Nanocomposite Photocatalysts

In our previous study [32], we discussed the following two plausible reaction channels for OH radical formation during the photocatalytic reduction of H_2O_2 on visible-light-irradiated plasmonic Au–TiO_2 photocatalysts: the direct reduction channel (3) and indirect reduction channel via superoxide anion radical (O_2^-) formation (4).

$$\text{Au-TiO}_2 + \text{hv} \rightarrow \text{e}^- + \text{positive charge in Au} \quad (1)$$

$$\text{e}^- + \text{O}_2 \rightarrow \text{O}_2{}^- \quad (2)$$

$$\text{H}_2\text{O}_2 + \text{O}_2{}^- \rightarrow \text{OH}^- + \text{OH} + \text{O}_2 \quad (3)$$

$$\text{H}_2\text{O}_2 + \text{e}^- \rightarrow \text{OH}^- + \text{OH} \quad (4)$$

The mechanism of OH radical formation was investigated by degassing oxygen gas using nitrogen gas. The influence of the amount of OH radicals formed by the irradiation of plasmonic Au–TiO_2 photocatalytic powders was also discussed. If OH radicals were generated via reaction (3), degassing oxygen would inhibit OH radical generation because reaction (3) involves the superoxide radical ($O_2{}^-$), which is formed by the photocatalytic reduction of oxygen molecules. We observed that the degassing of oxygen reduced the amount of 7-hydroxycoumarin because coumarin reacts with OH radicals; however, the ratios of decrease were not less than half regardless of the use of commercially available TiO_2 powders in the plasmonic Au–TiO_2 photocatalysts. Thus, we concluded that the main channel for OH radical formation during the plasmonic Au–TiO_2 photocatalyst-induced photocatalytic reduction of H_2O_2 is reaction (4).

In the present study, the degassing of oxygen was performed for the visible-light-irradiated bare $BiVO_4$ photocatalysts and $BiVO_4$–TiO_2 nanocomposite photocatalysts. To remove oxygen from the photocatalytic reaction system, a flow of N_2 gas was used in a closed glass flow photocatalytic reactor. To ensure the complete removal of oxygen from the reaction system, N_2 gas was flowed for more than 5 min before initiating the photocatalytic reaction through irradiation. Moreover, a dissolved oxygen meter was used to determine the amount of dissolved oxygen in the coumarin solution, in which the bare $BiVO_4$ and $BiVO_4$–TiO_2 nanocomposite photocatalytic films were immersed.

The results of these experiments are shown in Figure 6. For comparison, the visible-light-irradiated $BiVO_4$ and the UV (365 nm)-irradiated $BiVO_4$ photocatalytic films were investigated, and the results are shown in Figure 6.

For the UV- and visible-light-irradiated $BiVO_4$ photocatalytic films, oxygen degassing increased the amount of OH radicals because of the inhibition of $O_2{}^-$ formation, which facilitated the direct photocatalytic reduction of H_2O on the $BiVO_4$ surface via the reaction channel of Equation (4).

In contrast, for the visible-light-irradiated $BiVO_4$–TiO_2 nanocomposite photocatalysts, oxygen degassing decreased the amount of OH radicals. If OH radicals were formed via reaction (4), degassing oxygen would enhance OH radical formation because of the inhibition of $O_2{}^-$ formation. Thus, for visible-light-irradiated $BiVO_4$–TiO_2 nanocomposite photocatalysts, oxygen plays an important role in OH radical formation. For $BiVO_4$–TiO_2 nanocomposite photocatalysts, OH radicals were also formed by the reaction of Equation (3). This reaction, of Equation (3), known as the Haber–Weiss Reaction [37], occurred after the photoexcitation of the $BiVO_4$–TiO_2 forming $O_2{}^-$. During the electron migration from $BiVO_4$ to TiO_2, photoexcited electrons might be captured in the trapped sites in the $BiVO_4$–TiO_2 nanocomposite photocatalysts, and such trapping processes in the visible-light-irradiated $BiVO_4$–TiO_2 nanocomposite photocatalysts might cause such a difference in the mechanism of OH radical formation. The results are presented in Figure 7. According to our previous study [32], the main channel for OH radical formation during plasmonic Au–TiO_2-induced reduction of H_2O_2 is the direct photocatalytic reduction of H_2O on the $BiVO_4$ surface via the reaction channel of Equation (4).

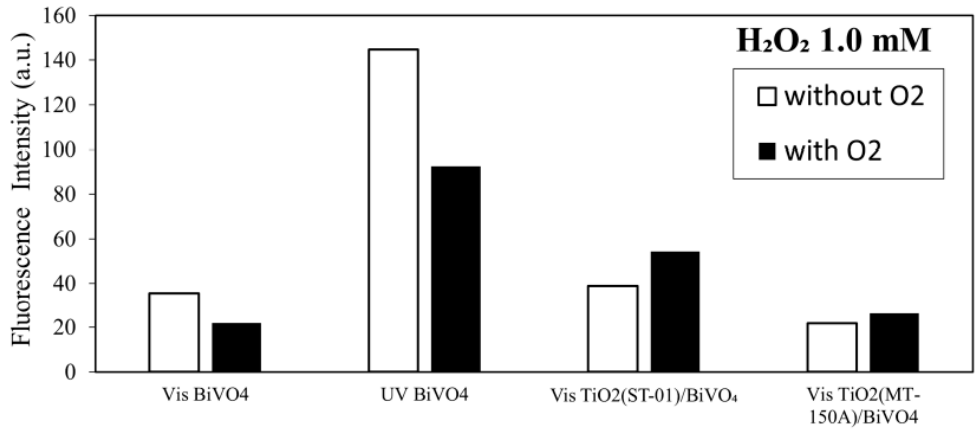

Figure 6. Effect of oxygen degassing on the fluorescence intensity of 7-hydroxycoumarin formed during the photocatalytic reaction on the visible-light-irradiated (LED, λ = 470 nm) $BiVO_4$–TiO_2 (ST-01: Anatase) and $BiVO_4$–TiO_2 (MT-150A: Rutile) nanocomposite photocatalytic films. These films were immersed in 0.15 mM coumarin aqueous solution. For comparison, the effect of oxygen degassing on the fluorescence intensity of 7-hydroxycoumarin formed during the photocatalytic reactions on visible-light-irradiated $BiVO_4$ films (LED, λ = 470 nm) and UV-light-irradiated $BiVO_4$ films (LED, λ = 365 nm) in 0.15 mM coumarin aqueous solution was also investigated. For these fluorescence measurements, the Ti/Bi ratio for the $BiVO_4$–TiO_2 nanocomposite film used was fixed at 20:1. The concentration of H_2O_2 was fixed at 1 mM, and the excitation wavelength was set to 350 nm ((□) without O_2 (■) with O_2).

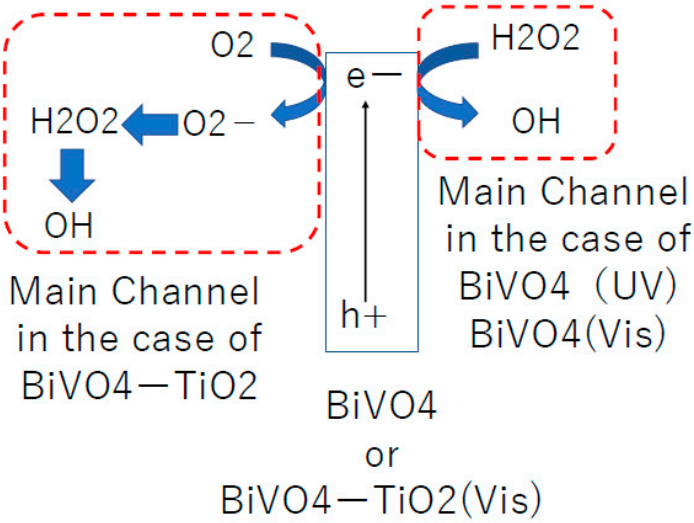

Figure 7. Schematic for the proposed mechanism for OH radical formation by H_2O_2 reduction on the $BiVO_4$ photocatalyst and the indirect mechanism for the reaction of O_2^- and H_2O_2 on the $BiVO_4$–TiO_2 nanocomposite photocatalyst.

Plasmonic Au–TiO_2 photocatalysts generate hot electrons in Au nanoparticles and inject them into the conduction band of TiO_2, as previously investigated by several researchers [38,39]. These hot electrons play key roles in OH radical formation via reaction channel (4). One plausible explanation for the difference in the reaction channels of OH radical formation from H_2O_2 between $BiVO_4$ and $BiVO_4$–TiO_2 nanocomposite photocatalysts is the distinct reactivities of the trapped and hot electrons. There are several discussions on the reaction rates [40] and reaction sites [41] of trapped electrons during molecular oxygen reduction on the conduction band of TiO_2 photocatalytic reactions. However, no studies have investigated the different reactivities of free and trapped electrons in the photocatalytic reduction of H_2O_2. However, Losada et al. [42] used density functional

theory to study the reaction of H_2O_2 with the surface of a transition metal oxide. There have been several previous discussions on whether OH radicals are formed by the reduction of H_2O_2 via reaction channel (4). Nosaka et al. [43] concluded that reaction (4) did not occur during the photocatalytic reaction of TiO_2. They determined the redox potential for reaction channel (4) as +0.73 V vs SHE at pH 7. Yu et al. [44] determined the redox potential for reaction channel (4) as +0.1 V vs SHE, which was close to the value reported by Nosaka et al. [43]. Because of the potential of the conduction band edge of $BiVO_4$, that of TiO_2 is more negative than the redox potential for reaction (4). Therefore, reaction (4) could proceed in the present reaction system containing the bare $BiVO_4$ photocatalytic film or $BiVO_4$–TiO_2 nanocomposite photocatalytic film under-visible light irradiation if only the redox potential is considered. These speculations remain unclear because of the lack of direct evidence, such as the detection of superoxide anions in the present photocatalytic reaction system. Recently, hydroxide-based co-catalysts for heterogeneous photocatalysis have been developed, and the authors have discussed enhanced electron migration and hydrogen evolution [45,46]. The use of other photocatalysts, such as hydroxide-based photocatalysts, may contribute to a better understanding of the roles of photocatalytic reduction channels in OH radical formation from H_2O_2 using $BiVO_4$–TiO_2 nanocomposite photocatalytic systems.

Further studies to detect other active oxygen or intermediate species, such as superoxide anion radicals, in the photocatalytic reaction system are necessary to clarify the mechanism proposed in this study.

4. Conclusions

We investigated the formation of OH radicals on visible-light-responsive $BiVO_4$ nanocomposite films mixed with commercially available TiO_2 particles. We observed that the amount of OH radicals formed by the photoexcited electron transfer from the visible-light-irradiated $BiVO_4$ thin film to TiO_2 particles was independent of the particle size and crystal phase of TiO_2 except for two commercially available TiO_2 particles with primary particle sizes of less than 10 nm. The effects of H_2O_2 addition on OH radical formation were also examined to investigate the possible role of OH radical formation in the reduction reaction of H_2O_2 on the surfaces of the $BiVO_4$–TiO_2 nanocomposite photocatalysts. An increase in the number of OH radicals with increasing H_2O_2 concentration was observed for the visible-light irradiated $BiVO_4$–TiO_2 nanocomposite photocatalyst irrespective of the crystal phase of TiO_2 (anatase or rutile). The amount of OH radicals formed by the visible-light irradiation of the $BiVO_4$ film photocatalyst was much smaller than that formed by the visible-light irradiation of the $BiVO_4$–TiO_2 nanocomposite film photocatalyst. This indicates that the electron transfer from $BiVO_4$ to TiO_2 suppressed the charge recombination reaction of electrons and holes in the $BiVO_4$–TiO_2 nanocomposite thin-film photocatalyst. In addition, we observed that the ratio of the increase in the amount of OH radicals upon adding H_2O_2 to the visible-light-irradiated $BiVO_4$–TiO_2 nanocomposite photocatalysts was smaller than that of the $BiVO_4$ photocatalytic film. We also discussed the reduction potentials of the $BiVO_4$ thin-film photocatalyst and $BiVO_4$–TiO_2 nanocomposite photocatalyst under visible-light irradiation.

Next, we confirmed the role of oxygen in OH radical formation during the photocatalytic reduction of H_2O_2 on the $BiVO_4$–TiO_2 nanocomposite film under visible light irradiation. Oxygen degassing was also performed for the visible-light-irradiated $BiVO_4$ and $BiVO_4$–TiO_2 nanocomposite films. Different mechanisms were suggested for OH radical formation during the photocatalytic reduction reaction of H_2O_2 in the presence of visible-light-irradiated bare $BiVO_4$ and $BiVO_4$–TiO_2 photocatalytic films. In the present study, measurements of the superoxide radicals (O_2^-) were not carried out. As superoxide radicals are one of the key species in the photocatalytic reduction reaction, measurements of other intermediates, such as O_2^-, would help in understanding the mechanism.

Author Contributions: Y.M., writing and editing; S.T., formal analysis and investigation. All authors have read and agreed to the published version of the manuscript.

Funding: This study received no external funding.

Data Availability Statement: The data presented in this study are available upon request from the corresponding author.

Conflicts of Interest: The authors declare no conflicts of interest.

References

1. Kudo, A.; Omori, K.; Kato, H. A Novel Aqueous Process for Preparation of Crystal Form-Controlled and Highly Crystalline $BiVO_4$ Powder from Layered Vanadates at Room Temperature and Its Photocatalytic and Photophysical Properties. *J. Am. Chem. Soc.* **1999**, *121*, 11459–11467. [CrossRef]
2. Zhang, Z.; Wang, W.; Shang, M.; Yin, W. Photocatalytic degradation of rhodamine B and phenol by solution combustion synthesized $BiVO_4$ photocatalyst. *Catal. Commun.* **2010**, *11*, 982–986. [CrossRef]
3. Huang, C.; Chen, L.; Li, H.; Mu, Y.; Yang, Z. Synthesis and application of Bi_2WO_6 for the photocatalytic degradation of two typical fluoroquinolones under visible light irradiation. *RSC Adv.* **2019**, *9*, 27768–27779. [CrossRef] [PubMed]
4. Ai, Z.; Huang, Y.; Lee, S.; Zhang, L. Monoclinic α-Bi_2O_3 photocatalyst for efficient removal of gaseous NO and HCHO under visible light irradiation. *J. Alloys Compd.* **2011**, *509*, 2044–2049. [CrossRef]
5. Tang, J.; Zou, Z.; Ye, J. Efficient Photocatalytic Decomposition of Organic Contaminants over $CaBi_2O_4$ under Visible-Light Irradiation. *Angew. Chem.* **2004**, *116*, 4563–4566. [CrossRef]
6. Murakami, Y.; Chatchai, P.; Nosaka, Y. Developments of the Efficient Water-splitting Electrodes under the Visible Light Irradiation. *Electrochemistry* **2009**, *77*, 44–50. [CrossRef]
7. Stelo, F.; Kublik, N.; Ullah, S.; Wender, H. Recent advances in Bi_2MoO_6 based Z-scheme heterojunctions for photocatalytic degradation of pollutants. *J. Alloys Compd.* **2020**, *829*, 154591. [CrossRef]
8. Abdi, F.; Savenije, T.J.; May, M.M.; Dam, B.; Krol, R. The Origin of Slow Carrier Transport in $BiVO_4$ Thin Film Photoanodes: A Time-Resolved Microwave Conductivity Study. *J. Phys. Chem. Lett.* **2013**, *4*, 2752–2757. [CrossRef]
9. Ziwritsch, M.; Muller, S.; Hempel, H.; Unold, T.; Abdi, F.F.; Krol, R.; Friedrich, D.; Eichberger, R. Direct Time-Resolved Observation of Carrier Trapping and Polaron Conductivity in $BiVO_4$. *ACS Energy Lett.* **2016**, *1*, 888–894. [CrossRef]
10. Hu, Y.; Li, D.; Zheng, Y.; Chem, W.; He, Y.; Shao, Y.; Fu, X.; Xiao, G. $BiVO_4/TiO_2$ nanocrystalline heterostructure: A wide spectrum responsive photocatalyst towards the highly efficient decomposition of gaseous benzene. *Appl. Catal. B Environ.* **2011**, *104*, 30–36. [CrossRef]
11. Zhang, L.; Tan, G.; Wei, S.; Ren, H.; Xia, A.; Luo, Y. Microwave hydrothermal synthesis and photocatalytic properties of $TiO_2/BiVO_4$ composite photocatalysts. *Ceram. Int.* **2013**, *39*, 8597–8604. [CrossRef]
12. Wetchakun, N.; Chainset, S.; Phanichphant, S.; Wetchakun, K. Efficient photocatalytic degradation of methylene blue over $BiVO_4/TiO_2$ nanocomposites. *Ceram. Int.* **2014**, *41*, 5999–6004. [CrossRef]
13. Song, X.; Li, Y.; Wei, Z.; Ye, S.; Dionysiou, D. Synthesis of $BiVO_4$/P25 composites for the photocatalytic degradation of ethylene under visible light. *Chem. Eng. J.* **2017**, *314*, 443–452. [CrossRef]
14. Ho-Kimura, S.; Moniz, S.J.A.; Handko, A.D.; Tang, J. Enhanced photoelectrochemical water splitting by nanostructured $BiVO_4$–TiO_2 composite electrodes. *J. Mater. Chem. A* **2014**, *2*, 3948–3953. [CrossRef]
15. Resasco, J.; Zhang, H.; Kornienko, N.; Becknell, N.; Lee, H.; Guo, J.; Briseno, A.L.; Yang, P. $TiO_2/BiVO_4$ Nanowire Heterostructure Photoanodes Based on Type II Band Alignment. *ACS Cent. Sci.* **2016**, *2*, 80–88. [CrossRef] [PubMed]
16. Cheng, B.; Yang, J.; Cho, H.; Wu, J. Fabrication of an Efficient $BiVO_4$–TiO_2 Heterojunction Photoanode for Photoelectrochemical Water Oxidation. *ACS Appl. Mater. Interfaces* **2016**, *8*, 20032–20039. [CrossRef] [PubMed]
17. Polo, A.; Grigioni, I.; Dozzi, M.; Selli, E. Sensitizing effects of $BiVO_4$ and visible light-induced production of highly reductive electrons in the $TiO_2/BiVO_4$ heterojunction. *Catal. Today* **2020**, *340*, 19–25. [CrossRef]
18. Kohtani, S.; Tomohiro, M.; Tokumura, K.; Nakagaki, R. Photooxidation reactions of polycyclic aromatic hydrocarbons over pure and Ag-loaded $BiVO_4$ photocatalysts. *Appl. Catal. B. Environ.* **2005**, *58*, 265–272. [CrossRef]
19. Zhang, J.; Nosaka, Y. Generation of OH radicals and oxidation mechanism in photocatalysis of WO_3 and $BiVO_4$ powders. *J. Photochem. Photobiol. A Chem.* **2015**, *303–304*, 53–58. [CrossRef]
20. Liu, G.; Wum, T.; Zhao, J.; Hidaka, H.; Serpone, N. Photoassisted Degradation of Dye Pollutants. 8. Irreversible Degradation of Alizarin Red under Visible Light Radiation in Air-Equilibrated Aqueous TiO_2 Dispersions. *Environ. Sci. Technol.* **1999**, *33*, 2081–2087. [CrossRef]
21. Nosaka, A.Y.; Fujiwara, T.; Yagi, H.; Akutsu, H.; Nosaka, Y. Photoinduced Changes of Surface and Adsorbed Water in TiO_2 Photocatalytic Systems as Studied by Solid State ^{1}H-NMR Spectroscopy. *Chem. Lett.* **2002**, *31*, 420. [CrossRef]
22. Zhang, J.; Nosaka, Y. Mechanism of the OH Radical generation in Photocatalysis with TiO_2 of Different Crystalline Types. *J. Phys. Chem. C* **2014**, *118*, 10824–10832. [CrossRef]
23. Murakami, Y.; Endo, K.; Ohta, I.; Nosaka, A.Y.; Nosaka, Y. Can OH Radicals Diffuse from the UV-Irradiated Photocatalytic TiO_2 Surfaces? Laser-Induced-Fluorescence Study. *J. Phys. Chem. C* **2007**, *111*, 11339–11346. [CrossRef]
24. Deguchi, S.; Shibata, N.; Takeuchi, T.; Fujiwara, Y.; Isu, N. Photocatalytic Hydrogen Production from Aqueous Solution of Various Oxidizing Sacrifice Agents. *J. Jpn. Petroleum. Inst.* **2010**, *52*, 95–100. [CrossRef]

25. Louie, G.; Foley, S.; Cabilic, J.; Coffigny, H.; Taran, F.; Valleix, A.; Renault, J.P.; Pin, S. The reaction of coumarin with the OH radical revisited: Hydroxylation product analysis determined by fluorescence and chromatography. *Radiat. Phys. Chem.* **2005**, *72*, 119–124. [CrossRef]
26. Zhang, J.; Nosaka, Y. Quantitative detection of OH radicals for investigating the reaction mechanism of Various visible-light TiO_2 photocatalysts in aqueous suspension. *J. Phys. Chem. C* **2013**, *117*, 1383–1391. [CrossRef]
27. Dibbel, R.S.; Watson, D.F. Distance-Dependent Electron Transfer in Tethered Assemblies of CdS Quantum Dots and TiO_2 Nanoparticles. *J. Phys. Chem. C* **2009**, *113*, 3139–3149. [CrossRef]
28. Du, L.; Furube, A.; Yamamoto, K.; Hara, K.; Katoh, R.; Tachiya, M. Plasmon-Induced Charge Separation, and Recombination Dynamics in Gold-TiO_2 Nanoparticle Systems: Dependence on TiO_2 Particle Size. *J. Phys. Chem. C* **2009**, *113*, 6454–6462. [CrossRef]
29. Liu, S.; Jaffrezic, N.; Guillard, C. Size effects in liquid-phase photo-oxidation of phenol using nanometer-sized TiO_2 catalysts. *Appl. Surf. Sci.* **2008**, *255*, 2704–2709. [CrossRef]
30. Wu, T.; Liu, G.; Zhao, J.; Hidaka, H.; Serpone, N. Evidence for H_2O_2 Generation during the TiO_2-Assisted Photodegradation of Dyes in Aqueous Dispersions under Visible Light Illumination. *J. Phys. Chem. B* **1999**, *103*, 4862–4867. [CrossRef]
31. Li, X.; Chen, C.; Zhao, J. Mechanism of Photodecomposition of H_2O_2 on TiO_2 surfaces under Visible Light Irradiation. *Langmuir* **2001**, *17*, 4118–4122. [CrossRef]
32. Hayashi, T.; Nakamura, K.; Suzuki, T.; Saito, N.; Murakami, Y. OH radical formation by the photocatalytic reduction reactions of H_2O_2 on the surface of plasmonic excited Au-TiO_2 photocatalysts. *Chem. Phys. Lett.* **2020**, *739*, 136958. [CrossRef]
33. Hirakawa, T.; Yawata, K.; Nosaka, Y. Photocatalytic reactivity for O_2 and OH radical formation in anatase and rutile TiO_2 suspension as the effect of H_2O_2 addition. *Appl. Catal. A Gen.* **2007**, *325*, 105–111. [CrossRef]
34. Nakabayashi, Y.; Nishikawa, M.; Saito, N.; Terashima, C.; Fujishima, A. Significance of Hydroxyl Radical in Photoinduced Oxygen Evolution in Water on Monoclinic Bismuth Vanadate. *J. Phys. Chem. C* **2017**, *121*, 25624–25631. [CrossRef]
35. Shi, L.; Xu, C.; Zhang, H.; Liu, Z.; Qu, X.; Du, F. Facile fabrication of hierarchical $BiVO_4/TiO_2$ heterostructures for enhanced photocatalytic activities under visible-light irradiation. *J. Mater. Sci.* **2018**, *53*, 11329–11342. [CrossRef]
36. Wang, Y.; Lu, N.; Luo, M.; Fan, L.; Zhao, K.; Qu, J.; Guan, J.; Yuan, X. Enhancement mechanism of fiddlehead-shaped TiO_2-$BiVO_4$ type II heterojunction in SPEC towards RhB degradation and detoxification. *Appl. Surf. Sci.* **2019**, *463*, 234–243. [CrossRef]
37. Kehrer, J.P. The Haber–Weiss reaction and mechanisms of toxicity. *Toxicology* **2000**, *149*, 43–50. [CrossRef] [PubMed]
38. Furube, A.; Du, L.; Hara, K.; Kato, R.; Tachiya, M. Ultrafast Plasmon-Induced Electron Transfer from Gold Nanodots into TiO_2 Nanoparticles. *J. Am. Chem. Soc.* **2007**, *129*, 14852–14853. [CrossRef]
39. Du, L.; Furube, A.; Hara, K.; Kato, R.; Tachiya, M. Ultrafast plasmon-induced electron injection mechanism in gold–TiO_2 nanoparticle system. *J. Photochem. Photobiol. C* **2013**, *15*, 21–30. [CrossRef]
40. Bahnemann, D.W.; Hilgendorff, M.; Memming, R. Charge Carrier Dynamics at TiO_2 Particles: Reactivity of Free and Trapped Holes. *J. Phys. Chem. B* **1997**, *101*, 4265–4275. [CrossRef]
41. Henderson, M.; Epling, W.S.; Peden, C.H.; Perkins, C.L. Insights into Photoexcited Electron Scavenging Processes on TiO_2 Obtained from Studies of the Reaction of O_2 with OH Groups Adsorbed at Electronic Defects on TiO_2(110). *J. Phys. Chem. B* **2003**, *107*, 534–545. [CrossRef]
42. Losada, C.M.; Johansson, J.; Brinck, T.; Jonsson, M. Mechanism of H_2O_2 Decomposition on Transition Metal Oxide Surfaces. *J. Phys. Chem. C* **2012**, *116*, 9533–9543. [CrossRef]
43. Nosaka, Y.; Nosaka, A.Y. Understanding Hydroxyl Radical (•OH) Generation Processes in Photocatalysis. *ACS Energy Lett.* **2016**, *1*, 356–359. [CrossRef]
44. Yu, T.; Breslin, C.B. Review—2D Graphene and Graphene-Like Materials and Their Promising Applications in the Generation of Hydrogen Peroxide. *J. Electrochem. Soc.* **2020**, *167*, 126502. [CrossRef]
45. Xie, L.; Hao, J.-G.; Chen, H.-Q.; Li, Z.-X.; Ge, S.-Y.; Mi, Y.; Yang, K.; Lu, K. Recent advances of nickel hydroxide-based cocatalysts in heterogeneous photocatalysis. *Catal. Commun.* **2022**, *162*, 106371. [CrossRef]
46. Wei, Y.; Hao, J.-G.; Zhang, J.-L.; Huang, W.-Y.; Ouyang, S.-B.; Yang, K.; Lu, K.-Q. Integrating $Co(OH)_2$ nanosheet arrays on graphene for efficient noble-metal-free EY-sensitized photocatalytic H_2 evolution. *Dalton. Trans.* **2023**, *52*, 13923–13929. [CrossRef]